Journal of Magnetic Resonance **136,** 37–46 (1999)
Article ID jmre.1998.1620, available online at http://www.idealibrary.com on IDEAL®

# A Comparison of 1D and 2D (Unbiased) Experimental Methods for Measuring CSA/DD Cross-Correlated Relaxation

Gy. Batta,* K. E. Kövér,* and J. Kowalewski†

*Research Group for Antibiotics of the Hungarian Academy of Sciences and Department of Organic Chemistry, L. Kossuth University, P.O. Box 70, H-4010 Debrecen, Hungary; and †Division of Physical Chemistry, Arrhenius Laboratory, Stockholm University, S-106 91 Stockholm, Sweden

Received July 14, 1998; revised September 22, 1998

**Conventional and enhanced 1D experiments and different NOESY experiments (the 2D unbiased method) were performed for measuring CSA/DD cross-correlated relaxation on trehalose, a compound which could be approximated as a spherical top, and on simple model compounds comprising $C_{3v}$ symmetry ($CHCl_3$, triphenylsilane (TPSi)). The comparison gives experimental evidence for the equivalence of the methods within the limits of the two-spin approach. 1D data are evaluated with both the simple initial rate and the Redfield relaxation matrix approach. The 2D data are obtained from the so-called transfer matrix using the Perrin–Gipe eigenvalue/eigenvector method. For the improved performance of the 2D method, an *X*-filtered (HHH) NOESY is suggested at the natural abundance of $^{13}C$ (or other dilute, low $\gamma$ species). Also, experimental parameters crucial for reliable CSA data are tested (e.g., the impact of insufficient relaxation delay). Error estimation is carried out for fair comparison of methods. Revised liquid state $^1H$ and $^{13}C$ ($^{29}Si$) CSA data are presented for chloroform and TPSi.** 

*Key Words:* **CSA/DD cross-correlated relaxation; unbiased method; 1D techniques; chloroform; triphenylsilane.**

## INTRODUCTION

During the past decade, we saw an increasing interest in obtaining chemical shift anisotropy (CSA) information from liquid state relaxation studies (*1–14*). In some cases, the CSA can be obtained from the field dependence of the spin–lattice relaxation rates (*15–19*). More often, one has to rely on measurements of cross-correlation or interference effects between the CSA and the dipole–dipole (DD) interactions or, as proposed very recently, on the effects of partial alignment of magnetically anisotropic molecules in the high magnetic field (*20*). One of the reasons for this interest can be connected to indications from theoretical (*21*), solid (*22*), and liquid state (*10–13*) NMR that $^{15}N$ and proton chemical shift tensors can act as sensitive indicators of H bonding, geometry of the NH bond axis, etc.

The CSA/DD interference arises as the off-diagonal elements in relaxation matrices, connecting the single-spin operators (such as $I_z$) and two-spin operators, such as $2I_zS_z$ (*23–25*). The interference terms are often small, but not negligible, compared to the dominant DD relaxation mechanism. For example, small molecules in the extreme narrowing regime with a few tens of picoseconds reorientation time may exhibit a cross-correlated relaxation rate on the order of 0.001–0.01 $s^{-1}$. Accurate measurements of these small rates which may require the suppression of background magnetization (one-spin order) are generally difficult, especially when indirect ($^1H$) detection schemes are used for obvious sensitivity reasons. In this study, we compare different schemes for measurements of the longitudinal CSA/DD interference terms for small molecules and indicate some potential problems that can occur in such measurements. In particular, we compare an "unbiased" two-dimensional technique (*4*, *7*, *25*) with some novel one-dimensional methods. The general features of the methods under consideration are presented in the next section and the following sections cover some examples of comparisons and applications.

## THE METHODS

All the methods discussed here are based on a treatment of an isolated two-spin system. The appropriate operator basis for the discussion of the longitudinal relaxation in such a spin system consists of $I_z$, $S_z$, and $2I_zS_z$. The relaxation is described by the equation system (*4*, *24*, *25*)

$$\frac{d}{dt}\begin{pmatrix}\langle I_z\rangle\\ \langle S_z\rangle\\ \langle 2I_zS_z\rangle\end{pmatrix} = -\begin{pmatrix}\rho_I & \sigma_{IS} & \delta_{I,IS}\\ \sigma_{IS} & \rho_S & \delta_{S,IS}\\ \delta_{I,IS} & \delta_{S,IS} & \rho_{IS}\end{pmatrix}\begin{pmatrix}\langle I_z\rangle - \langle I_z\rangle_{eq}\\ \langle S_z\rangle - \langle S_z\rangle_{eq}\\ \langle 2I_zS_z\rangle\end{pmatrix}. \qquad [1]$$

Throughout this paper we use the convention where the negative sign is separated from the **R** matrix in [1]. As a consequence, all diagonal elements are positive. The diagonal terms $\rho_I$, $\rho_S$, and $\rho_{IS}$ in the relaxation matrix are the intrinsic relaxation rates for the *I* and *S* one-spin orders and the two-spin order, respectively. If *S* is identified with a carbon-13 or silicon-29 spin and *I* with the proton directly bonded to it, then $\rho_S$ is identical to the spin–lattice relaxation rate, of the *S* spin under proton decoupling conditions. Analogously, $\rho_I$ corresponds to the relaxation rate of protons bonded to the *S* spin, measured under the conditions of *S* spin decoupling. The symbol $\sigma_{IS}$ is the cross-relaxation rate, related to the heteronuclear NOE. The two $\delta$ terms are the cross-correlated



1090-7807/99 $30.00

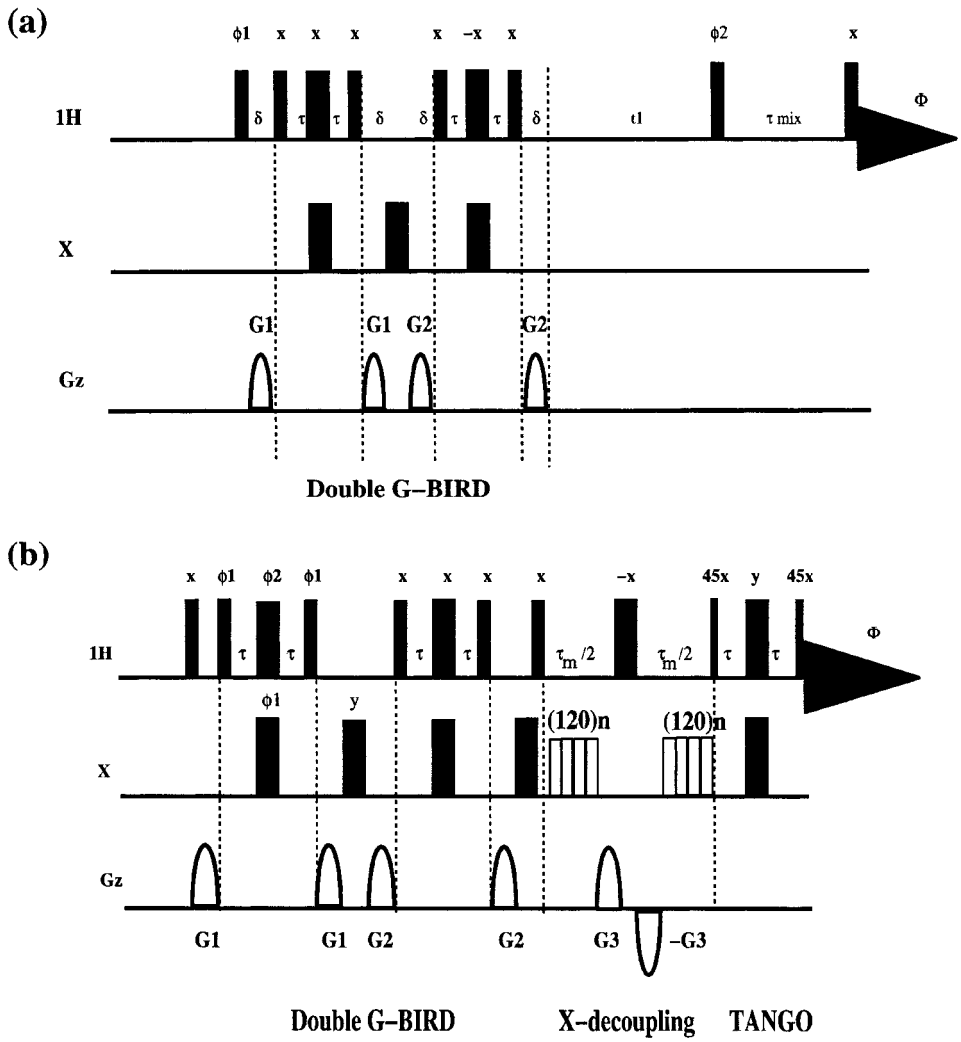


**FIG. 1.** The summary of the novel or modified experiments proposed in this study. Thin bars mean 90° and thick bars mean 180° hard pulses or the tip angle is given explicitly. Phases are $X$ if not indicated otherwise. Spin-lock pulses of preferably different durations last 2–3 ms at full power. The maximum gradient available was ca. 0.5 T/m (100%) and the amplitudes of sine bell-shaped gradients are given as a percentage of this value. (a) Proton NOESY with double G-BIRD $X(\omega_1)$ filter; $\phi1 = X_4\ -X_4$; $\phi2 = X\ -X\ -X\ X$; $\phi = X\ -X\ -X\ X\ -X\ X\ X\ -X$; and TPPI is applied for the first pulse. G1 and G2 gradients are 35 and 10, respectively. (b) $^1$H $T_1$ measurement in the $X$ satellite spectra with double G-BIRD and TANGO combination; $\phi1 = X\ Y\ -X\ -Y$; $\phi2 = -X\ -Y\ X\ Y$; $\phi = X\ -X$. $^{13}$C decoupling during relaxation is accomplished with a sequence of 120° (93 $\mu$s) carbon pulses. A 180° phase shift and 5-ms interpulse delay were applied after each decoupling pulse. Gradient amplitudes G1 = 11, G2 = 17, and G3 = 40 were applied. $T_1$ is obtained from a two-parameter exponential fit of the satellites. (c) The DQF–HOE experiment with decoupling during acquisition. $\phi1 = Y_2\ -Y_4\ Y_2$; $\phi2 = X_2\ -X_4\ X_2$; $\phi3 = X_4\ -X_4$; $\phi = \phi3$. For the reference experiment the second $^1$H 180° pulse is omitted, and the phase cycling is modified as $\phi1 = Y_4\ -Y_4$; $\phi2 = X_4\ -X_4$; $\phi3 = -X_4\ X_4$; $\phi = \phi1$. (d) The $X$-PT experiment utilizing the $\langle zz \rangle$ to $\langle z \rangle$ transfer: $\phi1 = Y_2\ -Y_4\ Y_2$; $\phi2 = Y_2\ -Y_2\ Y_2\ -Y_2\ -X_2\ X_2\ -X_2\ X_2$; $\phi3 = X_2\ -X_2\ X_2\ -X_2\ Y_2\ -Y_2\ Y_2\ -Y_2$; $\phi = X_4\ -X_4\ Y_4\ -Y_4$. The reference experiment is a standard refocused INEPT equipped with a 270° $X$ nucleus purging pulse just before the detection in concert with the receiver phase. (e) The proton-detected $X$-CSA experiment with INEPT preparation. $\phi1 = Y_8\ -Y_8$; $\phi2 = Y_8\ -Y_{16}\ Y_8$; $\phi3 = X_2\ -X_4\ X_2$; $\phi4 = X_4\ -X_4$ $\phi5 = Y_2\ -Y_4\ Y_2$; $\phi = X_4\ -X_4\ X_4\ -X_4\ -X_4\ X_4\ -X_4\ X_4$. (f) The proton-detected DQF–NOE experiment. $\phi1 = Y_2\ -Y_4\ Y_2$; $\phi2 = X_2, -X_4, X_2$; $\phi3 = X_4\ -X_4$; $\phi = \phi3$. In the reference experiment $\phi1 = Y_4\ -Y_4$ is used. Satellite intensities are measured in the presence of the parent $^1$H line. The same reference is useful for experiment e, since spin-lock times and other delays in the sequences are negligible compared to relaxation times.

(cc) relaxation rates. The measurement of these interference terms with concurrent techniques is the primary concern of this paper.

The "unbiased" 2D method is based on a series of three NOESY-type experiments using semiselective pulses: H-NOESY, $X$-NOESY, and HOESY (*26, 27*). The experiments have to be performed with zero (the reference experiments) and one or more nonzero mixing times. The approach is called unbiased, because the set of intensities of the diagonal, auto, and cross peaks of the $I$–$S$ doublets allows a unique reconstruction of the full relaxation matrix **R**. This algebraic eigenvalue/eigenvector method was originally introduced by Perrin and Gipe (*28*). A nonlinear fit of the six independent relaxation matrix elements to the measured multiplet component intensities is advantageous, since this procedure improves the statistics and allows the error estimation of the relaxation matrix elements (*7*).

In the one-dimensional longitudinal relaxation experi-

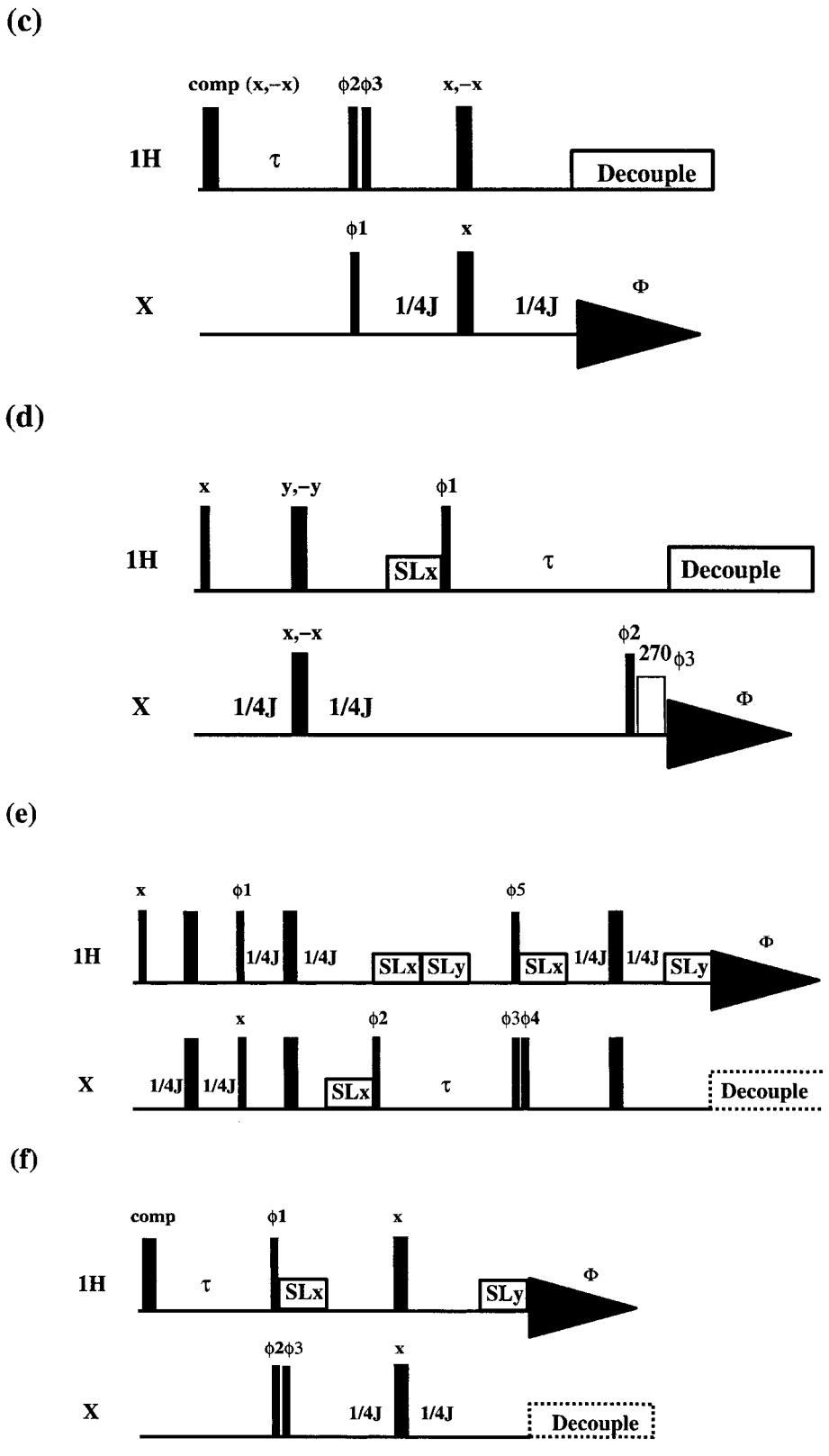


**FIG. 1**—*Continued*

ments, one observes relaxation-induced magnetization transfer between one-spin order ($\langle I_z \rangle$ or $\langle S_z \rangle$) and two-spin order ($2I_zS_z$). Initial, selective creation of a particular kind of order is followed by the mixing period. Then, another kind of order is observed during the detection period. A variety of such experiments were reviewed a few years ago

by Canet (*28*) and numerous varieties have been reported since then (*8*, *9*).

## EXPERIMENTAL

The sample of 1.7 M trehalose in $D_2O$ was identical to that used in our earlier work (*9*). The samples of triphenylsilane (7.5 mol% in toluene-$d_8$) and $^{13}CHCl_3$ (10 mol% carbon-13-enriched material in ethylene glycol-$d_8$) were the same as those used in previous studies (*4*, *7*).

The experiments on trehalose were performed on a Bruker DRX 500 spectrometer, operating at 11.8 T, using a 5-mm inverse detection gradient probe. The 90° pulse duration for the proton was 11 $\mu$s, while the corresponding duration for carbon-13 was 13.5 $\mu$s. The experiments on triphenylsilane were carried out on the same spectrometer, using a 10-mm broadband probe, with a proton 90° pulse of 34 $\mu$s and a silicon-29 90° pulse of 18 $\mu$s. In the experiments with proton or *X* nucleus decoupling, the WALTZ-16 scheme was applied at reduced power (ca. 100 $\mu$s for the 90° pulse). The power of the spin-lock pulses was the same as that for the hard pulses. The available pulsed field gradient amplitude was about 0.5 T $m^{-1}$. The experiments on the $^{13}CHCl_3$ sample were performed on a Varian Unity Plus 400 spectrometer, operating at 9.4 T, using a 10-mm broadband probe. The 90° pulse duration for proton and carbon-13 was 19 and 24 $\mu$s, respectively. In all cases, internal deuteron field/frequency lock was used and the temperature was controlled using the variable temperature controllers provided by the manufacturers. The pulse sequences proposed and applied in this study are presented in Fig. 1.

The spectral widths were typically 1.5–2 times the heteronuclear coupling constant or covered the required chemical shift range. The number of acquisitions varied between 4 and 64. Recycle delays of about 7–10 times the relevant $T_1$ (see the discussion of the chloroform data) were allowed. In the 2D experiment, the number of $t_1$ increments was typically 20–32 (TPSi) or 64–128 (trehalose). Measurement of 1D buildup curves (10–15 points) required 1 h (trehalose) or 17–24 h (TPSi) instrument time. The phase-sensitive NOESY data were acquired using the TPPI method. All the processing of the 1D and 2D spectra was performed using the spectrometer computers. The intensities of the 2D data were obtained by volume integration, after polynomial baseline correction in the H-NOESY experiment.

Nonlinear least-squares fitting of the 2D data was carried out using the program GENLSS (*30*) running on an IBM RISC 6000 workstation. The parameters fitted were all the relaxation matrix elements. The fitting of the 1D data was performed using the initial rate (double exponential fit or second order polynomial fit, followed by the calculation of the first derivative at the time origin) or using the method of Trudeau *et al.* (*31*), implemented with MATLAB software (*32*). The uncertainties of the parameters from the 1D experiments were estimated by the Monte Carlo method. The relative error estimates for the CSA from the Trudeau method were assumed to be proportional to the errors of the cross-correlation rates.

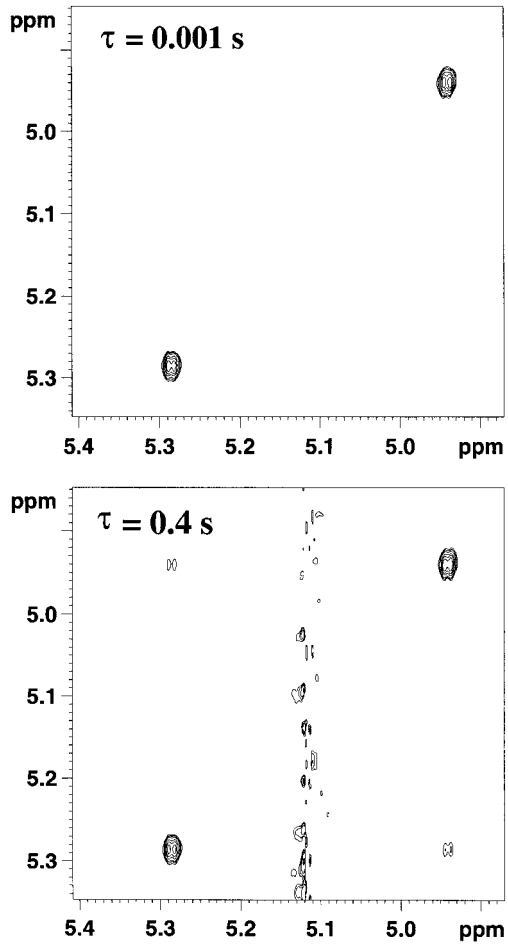


**FIG. 2.** The 2D NOESY proton spectra of the anomeric proton of trehalose as obtained using the sequence of Fig. 1a at mixing times of 0.001 and 0.4 s.

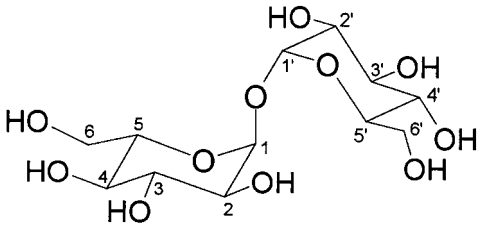


**SCHEME 1**

## TREHALOSE

We have recently presented a very detailed, temperature-dependent CSA study on a symmetric disaccharide called trehalose (*9*), Scheme 1. Based on earlier single-crystal NMR data (*33*) a "quasi"-cylindrical symmetry of the C-1 shift tensors in glucose rings is supposed. However, little is known about the $^1H$ CSA tensor in carbohydrates. Here, we compare the 1D results (at 300 K for the 1.7 M $D_2O$ solution) and the

new 2D data on the anomeric $^{13}C$–$^{1}H$ spin system at natural carbon-13 abundance. There are several reasons for choosing this particular system for the comparison of methods: one is that good quality 1D data and molecular dynamics were partly available. Another is that oligosaccharides are a class of small organic compounds subject to intense investigations by NMR relaxation methods (*5, 8, 9, 34–37*). Subtle details of their relaxation behavior—such as the cross-correlation effects—may be of general interest.

Since serious baseline problems at natural abundance may distort the $^{1}H$-NOESY integrals, we tested a modification of the proton NOESY sequence. The modified sequence, displayed in Fig. 1a, makes use of an $X(\omega_1)$ filter (*38*) with the double G-BIRD element (*39*). The sequence allows more accurate determination of the carbon-13 satellite volumes, since the strong parent $^{1}H$ line is suppressed. In order to compare the performance of the *X*-filtered and conventional NOESY, we ran a few pairs of control experiments at 0.4 s mixing time. We found that the $\delta_{H,HC}$ rates were more stable with the new method. Its application is invaluable if relatively small one-bond coupling and large-diameter NMR tubes cause the "foot" problem, i.e., when the bottom of the strong central signal overlaps with the weak satellites. A pair of the *X*-filtered $^{1}H$-NOESY spectra is shown in Fig. 2. The 2D experiments actually used were the $^{13}C$-NOESY, *X*-filtered $^{1}H$-NOESY, and the $^{13}C$–$^{1}H$ HOESY, using mixing times of 0, 0.2, 0.3, 0.4, and 0.5s. All data were normalized to the relevant zero-mixing time experiment. The nonlinear least-squares fit of the 2D data set resulted in the relaxation matrix elements collected in Table 1. We can note in the table that the relative uncertainties of the large diagonal elements obtained from the 2D data set are on the order of 1%. The absolute values of the standard deviation of the much smaller $\delta$ terms are similar, and they translate into larger (but still acceptable) relative errors of the cross-correlation rates.

A variety of different 1D experiments was combined to give the full set of the **R** matrix elements at natural abundance. The results are presented in Table 1. 1D measurement of the $^{1}H$ intrinsic relaxation rate $\rho_H$ in the $^{13}C$ satellite spectrum requires an extended *X* filtering with the TANGO (*40*) element, as shown in Fig. 1b. Our $T_1$ sequence incorporates *X* filtering both in the preparation and before detection; however, $^{13}C$ decoupling is not recommended during the acquisition. After the D-G-BIRD filter element an extra *X* nucleus inversion pulse is applied to restore the initial *z* magnetization. Then, the labeled $^{1}H$ magnetization is flipped to the $-z$ axis and is allowed to relax under *X* decoupling. In the middle of the mixing time a proton inversion pulse flanked by two opposite gradients provides a useful purging effect. Measurements of $\rho_C$ and $\sigma_{HC}$ were performed with standard methods, while the Ernst sequence (*41*) was used to obtain the decay rate for the two-spin order $\rho_{HC}$.

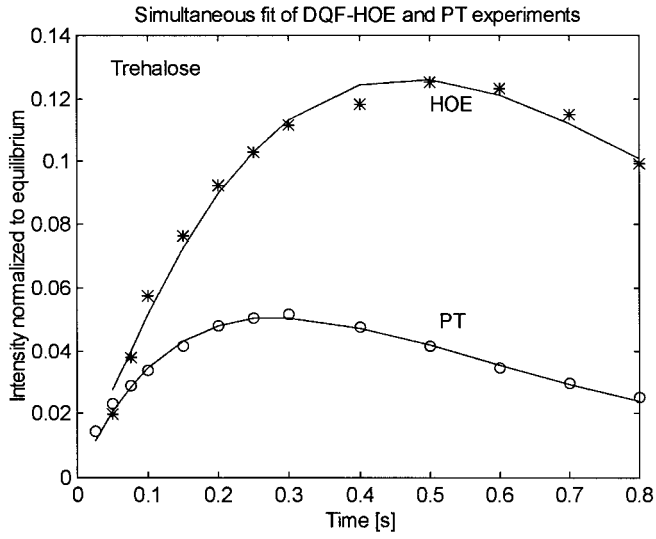


**FIG. 3.** The simultaneous fit of the buildup and decay curves from the proton and carbon CSA experiments for the anomeric C-1 carbon and proton of trehalose, obtained using the sequences of Figs. 1c and 1d.

**TABLE 1**

**The Relaxation Matrix R for the Anomeric C1, H1 System in Trehalose as Obtained by the "Unbiased" 2D and Different 1D Methods**

| Rate [$s^{-1}$] | 2D method | 1D initial rates | Applied 1D method |
|---|---|---|---|
| $\rho_H$ | 3.01 ± 0.03 | 3.07 ± 0.07 | $^{1}H$ $T_1$ (*X*-filtered) |
| $\sigma_{HC}$ | 0.69 ± 0.02 | 0.73 | HOE and $^{13}C$ $T_1$ |
| $\delta_{H,HC}$ | −0.10 ± 0.01 | −0.103 [−0.104] | DQF–HOE |
| $\rho_C$ | 3.48 ± 0.03 | 3.51 ± 0.02 | $^{13}C$ $T_1$ |
| $\delta_{C,HC}$ | 0.52 ± 0.02 | 0.53 [0.48] | $\langle zz\rangle$ to $\langle z\rangle$ |
| $\rho_{HC}$ | 3.72 ± 0.03 | 3.67 ± 0.04 | Ernst sequence (*41*) |

*Note.* The uncertainties in the 2D method correspond to one standard deviation of the nonlinear fit. The uncertainties in the diagonal elements of **R** in the 1D method are estimated from five to six repeated experiments. $\delta_{I,IS}$ and $\delta_{S,IS}$ cc rates in brackets were measured with gradient purging. The simultaneous fit of the $^{13}C$ and $^{1}H$ CSA experiments with the method of Trudeau *et al.* (*31*) is discussed in the text.

The $\delta_{H,HC}$ and $\delta_{C,HC}$ cc rates shown in the second column of Table 1 are the *initial rates* from $^{13}C$-detected 1D experiments. They are based on the double-quantum-filtered transient heteronuclear NOE (DQF–HOE, Fig. 1c) and the $\langle zz\rangle$ to $\langle z\rangle$ polarization transfer-enhanced (*X*-PT, Fig. 1d) experiments. We can see that the 2D and 1D rates agree well with each other. Simultaneous fit of the full buildup curves (Fig. 3) with the Trudeau method (*31*) using the known effective correlation time of 482 ps yields the geometry-dependent chemical shift anisotropy terms as CSAg($^{13}C$) = +27.6 ± 0.9 ppm and CSAg($^{1}H$) = −2.9 ± 0.2 ppm. It is important to point out that the CSA means chemical shift anisotropy, which has the opposite sign compared to the shielding anisotropy. The CSAg convention means geometry-dependent CSA term, e.g., when the angle subtended by the CSA tensorial axis and the *X*–H vector is not known *a priori*, and the angle is arbitrarily set to zero. From the same fit, we found that the random field contribution is negligible for C-1 ($A = -0.1 \pm 0.1\ s^{-1}$) but

is comparable to the interference terms for H-1 ($B = +0.6 \pm 0.1\ s^{-1}$). The confidence limit of the error estimates is 90% as calculated by the Monte Carlo method from 250 randomized "experiments." Using the 1D initial rates we arrive at CSAg($^{13}$C) = +28.4 ppm and CSAg($^{1}$H) = −4.2 ppm. The significant difference in $^{1}$H CSA values may be explained by the breakdown of the two-spin approach at longer mixing times. This is not surprising, since H-1 is exposed to dipolar interactions with H-2 and H-1′. Though we do not present the transversal measurements here, it is worth mentioning that we obtained CSAg($^{13}$C) = +29 ppm in the rotating frame $^{1}$H-detected 1D "ortho-ROESY" experiment (*42, 43*).

## IMPROVED LIQUID STATE CSA DATA FOR CHLOROFORM ($^{13}CHCl_3$)

Chloroform is a simple molecule, which can be studied by both theoretical and experimental methods. This is because $C_{3v}$ symmetry warrants an axially symmetric CSA tensor. Moreover, the symmetry axis is collinear with the principal axis of the DD interaction. Since published experimental data do have large scatter, we started a refined 1D cc study in order to lower the experimental uncertainties. The "unbiased" 2D experiments for establishing proton and carbon chemical shift anisotropy of chloroform were published by Mäler and Kowalewski (*4*). The carbon CSA results from that work, (+32 ± 8) ppm, deviated substantially from the data obtained in liquid crystalline solutions (*44, 45*) (+39 ± 1) or (+51.6 ± 0.2) ppm. To the contrary, the proton CSA data were in better agreement with each other: (−12 ± 2) ppm from 2D and (−9.8 ± 2.5) ppm from the liquid crystal study. More recently, the CSA in chloroform was also studied by *ab initio* quantum chemistry, and the results agreed best with one set of data measured in liquid crystal (*45*). Levitt and Di Bari introduced a new, steady-state cc method (*46*), and reported $\delta_{C,HC} = 13.7 \times 10^{-3}\ s^{-1}$ under identical experimental conditions (4.7 T and 300 K) as described in (*4*). Using the known 18-ps correlation time and the 107.3-pm CH distance, their data translate to CSA($^{13}$C) = +39.1 ppm. This time we used again the same sample as in the earlier 2D work (*4*). We ran the simplest double-quantum-filtered (DQF) inversion recovery sequences, starting with either $^{13}$C (*47*) or $^{1}$H (*8*) inversion pulses, and, unlike in the case of trehalose, without decoupling. As a possible source of error in the earlier 2D study, we suspected that the recycle delay might have been too short. From the diagonal elements of the **R** matrix obtained in the 2D experiments, the $^{1}$H and $^{13}$C relaxation times are both about 2.5 s at any of the applied fields (4.7 and 9.4 T). The recycle delay in the old experiments was 14 s. Now we carried out the 1D experiments at 9.4 T using recycle delays of 14, 22, and 35 s. The evolution of the resulting antiphase $^{13}$C doublets was evaluated using a simple initial rate method as described recently (*8, 9*). Artificial zero points were not applied to substitute zero evolution time experiments. In the 1D $^{13}$C CSA experiments, we observed a distortion of the amplitudes of the signals at short evolution

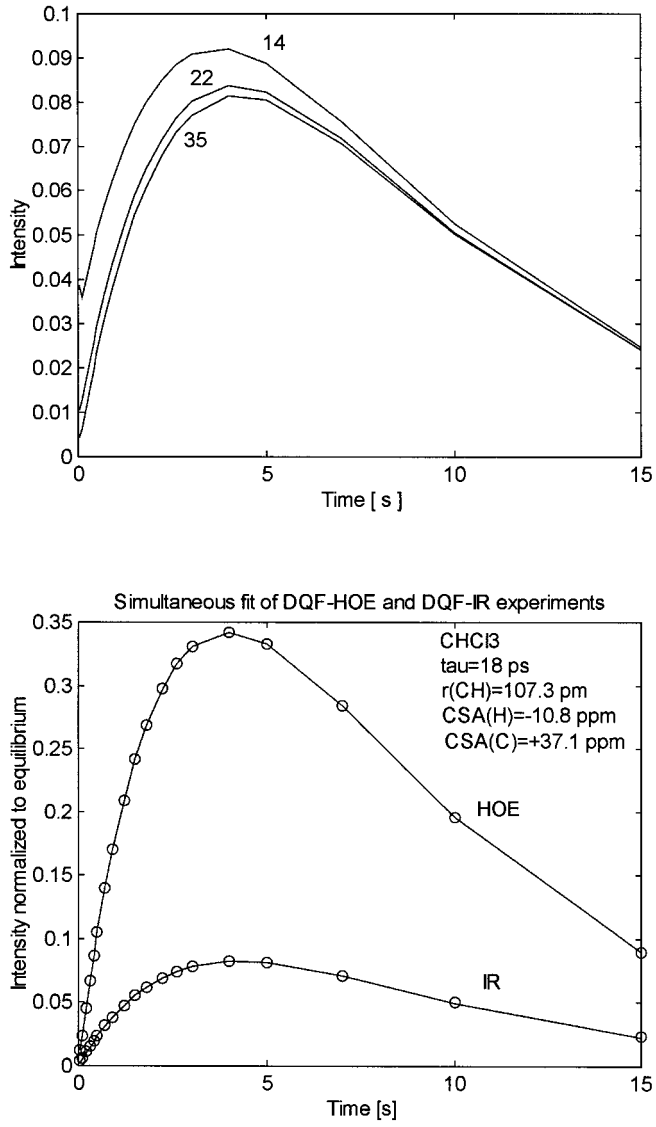


**FIG. 4.** The carbon CSA experiments for chloroform for different recycle delays of 14, 22, and 35 s as labeled on the upper part of the figure. The lower part shows the simultaneous fit of the DQF inversion recovery experiments starting with either $^{1}$H or $^{13}$C inversion.

times, which was drastically reduced when the long recycle delays were applied. Also, a small phase drift was observed as a function of the evolution time, but this effect was too small for influencing CSA data. Using the initial rates for the three series of the $^{13}$C CSA 1D experiments, the following cross-correlated relaxation rates and derived $^{13}$C CSA values were obtained: $\delta_{C,HC} = 20.8, 24.5, 25.3 \times 10^{-3}\ s^{-1}$; CSA($^{13}$C) = +29.8, +35.1, +36.2 ppm. We judge the experiment with the longest delay as the most reliable. It is obvious from the buildup curves shown in Fig. 4 that the initial rate period is the least distorted when the longest recycle delay is used. The DQF–HOE experiments are less sensitive to the length of the recycle delay in the initial period, although they also exhibited amplitude distortions. The resulting interference terms and the

CSA values are as follows: $\delta_{HCH} = -30.6, -30.1, -29.9 \times 10^{-3}$ s$^{-1}$, CSA($^1$H) = $-11.0$, $-10.8$, $-10.8$ ppm. The high-quality simultaneous fit of the two longest delay experiments is also shown in Fig. 4. Indeed, Monte Carlo error analysis proves the low errors, and we suggest revised liquid state values as CSA($^{13}$C) = $+37.1 \pm 0.25$ and CSA($^1$H) = $-10.85 \pm 0.02$. An estimated correlation time error (5–10%) may be added to these figures. The time constants for the decay rates of the two-spin order are the same in both experiments (ca. 3.5 s). As a conclusion, in both one- and two-dimensional experiments relevant to interference effects, we recommend a recycle delay of ca. 10 times the $\langle zz \rangle$ order decay time. Thus, the new measurements bring the CSA values in chloroform into closer agreement with most NMR data, except for one case measured in a liquid crystalline medium. The remaining discrepancies between the refined experimental (as well as theoretical) data may arise from different experimental conditions (e.g., solvent effects) and possibly from the scatter of "constants" (e.g., bond length).

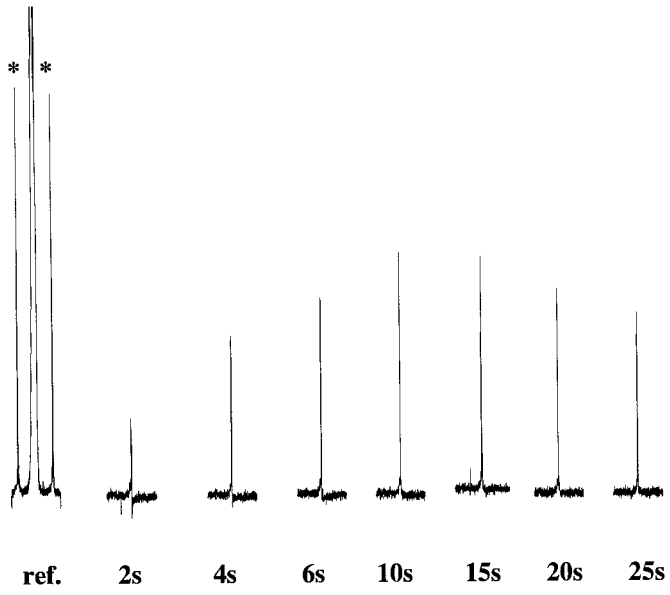


**FIG. 5.** The buildup of the $^{29}$Si CSA interference signals in the $^{29}$Si-detected (Fig. 1d) experiment, compared to the intensity of the one-bond carbon satellite. The first partial spectrum shows the reference experiment, a strong parent $^{29}$Si signal with its $^{13}$C satellites.

## TRIPHENYLSILANE: COMPARISON OF HIGH-FIELD 1D AND 2D RESULTS

The $^{29}$Si spin in triphenylsilane (TPSi) constitutes, together with its directly bonded proton ($^1J_{Si,H} = -198$ Hz), a pseudo two-spin system. This means that the dipolar interactions of this proton with the phenyl rings are neglected. Similarly, we neglect the $^{13}$C satellites arising from the resolved silicon–carbon couplings, $^1J = -70$ Hz, $^2J = 4.3$ Hz, and $^3J = -5.0$ Hz. Because of symmetry, in total, the satellites contribute as much as $15 \times 1.1 = 16.5\%$ of the full integral of the silicon signal. Fortunately, the *intensity* of the parent silicon signal in the $^1$H-decoupled spectra is not seriously affected. The silicon-29 nucleus relaxes very slowly, with the $T_1$ around 22 s, and this fact by itself is a challenge. Two-dimensional experiments for establishing proton and silicon chemical shift anisotropy in TPSi were reported earlier (*7*). The published results are CSA($^1$H) = $8 \pm 4$ ppm and CSA($^{29}$Si) = $-20 \pm 15$ ppm. The solid state measurements for silicon led to CSA($^{29}$Si) = $-40$ ppm (*7*). To resolve this contradiction, perhaps due to the low sensitivity at 4.7 T magnetic field, we ran both 1D and 2D experiments on the same liquid sample at 11.8 T.

In order to increase the sensitivity of the *X*-CSA methods, the polarization transfer technique combined with $^1$H decoupling during acquisition was applied as shown in Fig. 1d. However, since the effects are extremely small for silicon ($<3 \times 10^{-3}$ s$^{-1}$), in addition to the spin-lock purging of the antiphase proton magnetization, a self-refocusing silicon purging pulse proved to be useful before the detection. The advantage of this latter improvement is that it removes the dispersion component from the detected signal, and greatly improves the performance in the critical initial rate period. Figure 5 shows how small the real $^{29}$Si CSA effects are with respect to the intensity of the ca. 1.6% $^{13}$C satellite. Alternatively, $B_0$ field gradient pulses of different strengths may be applied in the beginning of the mixing period and before the final *X* read pulse. Higher sensitivity can be gained when the proton detection is used for the *X*-CSA measurement. The pulse sequence shown in Fig. 1e starts with a refocused INEPT to prepare an enhanced inverted *X* magnetization. Then, the orthogonal proton spin-lock pulses efficiently suppress the background $^1$H magnetization. In spite of the additional purging pulses and refocusing, the *X* nucleus decoupling during acquisition is impractical for TPSi, since suppression rates higher than $10^5$ are beyond the possibilities of the present technology. For the silicon CSA measurement, we evaluated the intensities for both the $^{29}$Si satellites in the refocused, undecoupled $^1$H spectra. Figure 6 demonstrates the scattered suppression of the parent proton signal in the Fig. 1e type experiment; still, the satellites could be quantitatively evaluated.

For the proton CSA measurements using *X* detection (DQF–HOE, Fig. 1c), the refocusing of the antiphase *X* doublets and proton decoupling during the *X* nucleus acquisition is quite straightforward. In the proton-detected variant of the DQF inversion recovery experiment (Fig. 1f), we again have the useful spin lock for purging the proton magnetization. However, the application of *X* decoupling after the refocusing period is generally not recommended for unlabeled compounds. The overlap with the center proton line could be safely avoided without decoupling, and a suppression rate of $3 \times 10^4$ was achieved. Generally, shorter proton $T_1$ is in favor of the proton detection and the sensitivity would be even higher with an inverse 10-mm probehead.

2D H-NOESY, *X*-NOESY, and HOESY experiments were carried out according to the original "unbiased" method using mixing times of 1 ms and 6, 8, and 10 s. We know from the

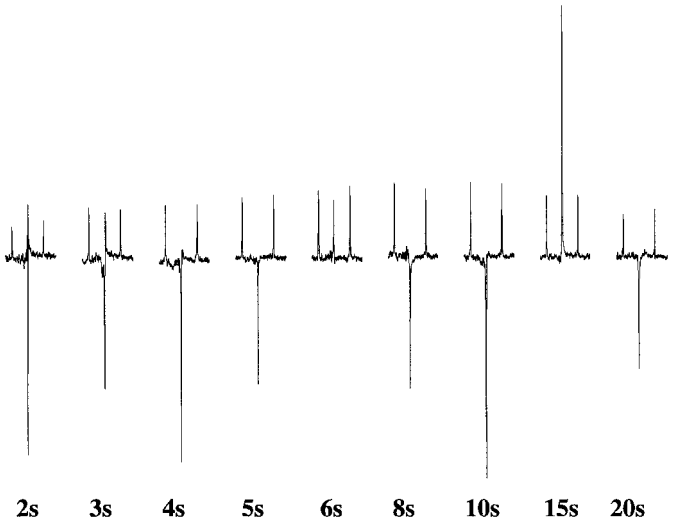


**FIG. 6.** The buildup of the $^{29}$Si CSA interference signals (silicon satellites) in the $^{1}$H-detected (Fig. 1e) experiment. The central $^{1}$H line is strongly attenuated; however, it exhibits a scatter due to experimental instabilities. As discussed in the text, such undecoupled spectra can be safely evaluated.

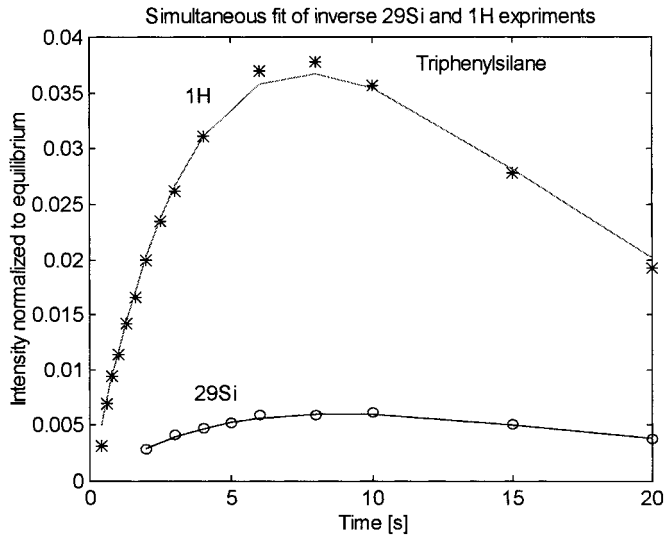


**FIG. 7.** The simultaneous fit of the $^{1}$H-detected $^{29}$Si and $^{1}$H CSA (Figs. 1e and 1f) experiments with the method of Trudeau *et al.* (*31*). Circles label the 1e and asterisks label the 1f experimental points. Numerical evaluation is discussed in the text.

earlier low-field work and the present 11.8-T measurements that the $T_1$ for silicon-29 is about 22 s and the rotational correlation time is close to 22 ps. In order to ensure reasonable experiment time, a 150-s recycle delay was inserted between each pulse sequence in 2D, and 200 s was allowed in the *X*-detected and 100 s in $^{1}$H-detected 1D experiments.

For comparing the efficiency of the 1D and 2D methods, it is advisable to compare the data obtained on the same spectrometer and sample. This comparison is shown in Table 2. The accuracy of the 2D data acquired at a field of 11.8 T appears in fact similar to the earlier 4.7-T (2D) results. The diagonal elements of the relaxation matrix differ slightly more than one standard deviation. Theoretically, the CSA/DD cross-correlated relaxation rates should be proportional to the external magnetic field. Indeed, the $\delta_{H,SiH}$ term increases with the field as expected. The extremely small $\delta_{Si,SiH}$ does not show any real change.

The low signal-to-noise ratio, due to the extremely small interference terms, does affect the initial rate approach. The signals are most distorted at the shortest mixing times, so occasional insertion of the 0,0 point in the fit may be useful. Also, the removal of the dispersion component of the detected signals at the data analysis stage can be applied. Disregarding the processing cosmetics, one might believe that the simultaneous fit of $^{1}$H and *X* experiments using the Trudeau *et al.* (*31*) method (cf. Table 2) would improve the accuracy, since it uses all points of the measured curves. The best signal-to-noise ratio was obtained in the $^{1}$H-detected experiments. Their simultaneous fit with the Trudeau method (Fig. 7) gives CSA($^{29}$Si) = $-7.4 \pm 0.3$ ppm and CSA($^{1}$H) = $+5.3 \pm 0.2$ ppm. With the correlation time of 22 ps, these correspond to the cross-correlated relaxation rates $\delta_{H,SiH}$ and $\delta_{Si,SiH}$ of $-6.6 \pm 0.3$ and $-1.8 \pm 0.1 \times 10^{-3}$ s$^{-1}$, respectively. The random field contributions ap-

**TABLE 2**
**The Relaxation Matrix for the $^{29}$SiH System of Triphenylsilane Obtained by the "Unbiased" 2D and by the Combination of Different 1D Methods**

| Rate parameter [$10^{-3}$ s$^{-1}$] | 2D rate at 4.7 T (Ref. *7*) | 2D rate at 11.8 T | 1D (initial) rates at 11.8 T, $^{29}$Si detection | 1D (initial) rates at 11.8 T, $^{1}$H detection |
|---|---|---|---|---|
| $\rho_H$ | 131 ± 3 | 153 ± 6 | — | — |
| $\sigma_{SiH}$ | 25 ± 2 | 23 ± 2 | 22.4 | — |
| $\delta_{H,SiH}$ | −4 ± 1 | −7 ± 2 | −7.5 (−7.2) | −6.8 |
| $\rho_{Si}$ | 60 ± 2 | 53 ± 3 | 46 | — |
| $\delta_{Si,SiH}$ | −2 ± 1 | −2 ± 1 | −1.8 (−2.0) | −2.0 |
| $\rho_{SiH}$ | 127 ± 1 | 117 ± 2 | — | — |

*Note.* The uncertainties in the 2D method correspond to one standard deviation of the fit. For the 1D methods, results of repeated measurements are labeled with parentheses. Note that since the rates are small, they are given in units of $10^{-3}$ s$^{-1}$ for better reading.

pear small ($<0.09\ s^{-1}$) but they still are one order of magnitude larger than the interference terms. The quality improvement in $^1$H-detected experiments is most remarkable when the silicon CSA is measured. As seen in Table 2, the $\delta_{H,SiH}$ rates are nearly identical in both the 1D and the 2D experiments. The $\delta_{Si,SiH}$ relative error estimates from the 2D data are large. The rates obtained in the different 1D experiments are, perhaps accidentally, less scattered. A simple algebraic average of the three independent 1D initial rates and the high-field 2D interference rates would lead to CSA($^{29}$Si) = $-7.8 \pm 0.5$ ppm and CSA($^1$H) = $+5.7 \pm 0.3$ ppm values, which agrees well with the result of the simultaneous fit. The significant difference between the solid and liquid state silicon chemical shift anisotropy in TPSi awaits an explanation. In the case of a related compound, triphenylmethane (TPM), the refined 1D experiments yielded CSA values comparable to the published 2D experiments (*7*), but the errors are smaller. The new data for TPM are CSA($^{13}$C) = $+7.2 \pm 0.5$ ppm and CSA($^1$H) = $-7.3 \pm 0.2$ ppm. In summary, the proposed 1D methods generally yield more accurate CSA data.

## CONCLUDING REMARKS

The comparison of the results obtained above deserves careful analysis. The "unbiased" 2D measurements provide the full relaxation matrix and the uncertainties of the small off-diagonal elements cannot be much smaller than those of the large diagonal rates. This results in a robust scheme, which has the ability to provide a correct estimate of all the rates simultaneously. If only a few elements of the **R** matrix are required, e.g., the cross-correlation rates, the use of specific 1D techniques is recommended.

Natural abundance detection of very small CSA requires special care in the experimental setup and in the data evaluation. If only the CSA is required, then the one-dimensional $^1$H-detected experiments are preferred, with a simultaneous fit of all the parameters to the buildup curves. This method also provides estimates of the random field contributions to relaxation. However, it needs an independent measurement of cross-relaxation rates, in order to obtain the dynamics necessary for CSA calculation. We found that in the case of a good signal-to-noise ratio and in the absence of multispin effects (*48*), the simple initial rate method (*47*) gives results comparable to those from simultaneous fitting.

## ACKNOWLEDGMENTS

This work has been supported by the Hungarian Grant OTKA T 014982 and the Swedish Natural Science Research Council. K.E.K. acknowledges support from Grant OTKA D 23749. General support from the Hungarian Ministry of Education (MKM-FKFP-0500/1997) is appreciated. Equipment grants for purchasing the DRX 500 spectrometer were provided by the OTKA A084, OMFB MEC 93-0098 and PHARE-ACCORD H-9112-0198 funds. Dr. L. Mäler is thanked for stimulating discussions.

## REFERENCES

1. T. C. Farrar and J. D. Decatur, *J. Phys. Chem.* **94,** 7395 (1990).
2. C. Dalvit, *J. Magn. Reson.* **95,** 410 (1991).
3. M. T. Chenon, C. Coupry, and L. G. Werbelow, *J. Phys. Chem.* **96,** 561 (1992).
4. L. Mäler and J. Kowalewski, *Chem. Phys. Lett.* **192,** 595 (1992).
5. L. Poppe and H. Van Halbeek, *Magn. Reson. Chem.* **31,** 665 (1993).
6. J. Bardakji, G. Kontaxis, H. Sterk, and R. Janoschek, *Spectrochim. Acta A* **50,** 735 (1994).
7. L. Mäler, L. Di Bari, and J. Kowalewski, *J. Phys. Chem.* **98,** 6244 (1994).
8. Gy. Batta and J. Gervay, *J. Am. Chem. Soc.* **117,** 368 (1995).
9. Gy. Batta, K. E. Kövér, J. Gervay, M. Hornyák, and G. M. Roberts, *J. Am. Chem. Soc.* **119,** 1336 (1997).
10. N. Tjandra, A. Szabo, and A. Bax, *J. Am. Chem. Soc.* **118,** 6986 (1996).
11. N. Tjandra and A. Bax, *J. Am. Chem. Soc.* **119,** 8076 (1997).
12. M. Tessari, F. A. A. Mulder, R. Boelens, and G. W. Vuister, *J. Magn. Reson.* **127,** 128 (1997).
13. M. Tessari, H. Vis, R. Boelens, R. Kaptein, and G. W. Vuister, *J. Am. Chem. Soc.* **119,** 8985 (1997).
14. N. Tjandra and A. Bax, *J. Am. Chem. Soc.* **119,** 9576 (1997).
15. J. J. Dechter and J. Kowalewski, *J. Magn. Reson.* **59,** 146 (1984).
16. D. Canet, J. B. Robert, and P. Tekely, *Chem. Phys. Lett.* **212,** 483 (1993).
17. P. Granger, J. Raya, J. Hirschinger, T. Richert, and K. El Bayed, *J. Chim. Phys. Phys-Chim. Biol.* **91,** 828 (1994).
18. T. C. Farrar, M. J. Jablonsky, and J. L. Schwartz, *J. Phys. Chem.* **98,** 4780 (1994).
19. K. T. Dayie and G. Wagner, *J. Am. Chem. Soc.* **119,** 7797 (1997).
20. M. Ottiger, N. Tjandra, and A. Bax, *J. Am. Chem. Soc.* **119,** 9825 (1997).
21. C. Facelli, R. J. Pugmire, and D. M. Grant, *J. Am. Chem. Soc.* **118,** 5488 (1996).
22. H. Wu, A. Ramamoorthy, L. M. Gierasch, and S. J. Opella, *J. Am. Chem. Soc.* **117,** 6148 (1995).
23. H. Shimizu, *J. Chem. Phys.* **40,** 3357 (1964).
24. M. Goldman, *J. Magn. Reson.* **60,** 437 (1984).
25. L. Di Bari, J. Kowalewski, and G. Bodenhausen, *J. Chem. Phys.* **93,** 7698 (1990).
26. P. L. Rinaldi, *J. Am. Chem. Soc.* **105,** 5167 (1983).
27. Chin Yu and G. C. Levy, *J. Am. Chem. Soc.* **105,** 6994 (1983); **106,** 6533 (1984).
28. L. Perrin and R. K. Gipe, *J. Am. Chem. Soc.* **106,** 4036 (1984).
29. D. Canet, *Prog. NMR Spectrosc.* **21,** 237 (1989).
30. F. DeTar, "Computer Programs for Chemistry," Vol. IV, Academic Press, New York (1972).
31. D. Trudeau, J. Bohmann, and T. C. Farrar, *J. Magn. Reson. A* **105,** 151 (1993).
32. MATLAB Reference Guide, Math Works, Natick, MA (1997).
33. M. H. Sherwood, D. W. Alderman, and D. M. Grant, *J. Magn. Reson. A* **104,** 132 (1993).
34. L. Mäler, G. Widmalm, and J. Kowalewski, *J. Phys. Chem.* **100,** 17103 (1996).
35. M. Hricovini and G. Torri, *Carbohydr. Res.* **268,** 159 (1995).

*36.* B. Engelsen, C. H. Du Penhoat, and S. Pérez, *J. Phys. Chem.* **99,** 13334 (1995).

*37.* A. Poveda, J. L. Asensio, M. Martin-Pastor, and J. Jiménez-Barbero, *J. Biomol. NMR* **10,** 29 (1997).

*38.* I. Furó, P. Mutzenhardt, and D. Canet, *J. Am. Chem. Soc.* **117,** 10405 (1995).

*39.* C. Emetarom, T. L. Hwang, G. Mackin, and J. Shaka, *J. Magn. Reson. A* **115,** 137 (1995).

*40.* S. Wimperis and R. Freeman, *J. Magn. Reson.* **58,** 348 (1984).

*41.* T. Bremi, M. Ernst, and R. R. Ernst, *J. Phys. Chem.* **98,** 9322 (1994).

*42.* R. Brüschweiler and R. R. Ernst, *J. Chem. Phys.* **96,** 1758 (1992).

*43.* Gy. Batta, K. E. Kövér, and J. Kowalewski, Applications of NMR to the study of the structure and dynamics of supramolecular complexes, NATO Advanced Research Workshop, Sitges (Barcelona), May 5–9, 1998.

*44.* P. K. Bhattacharyya and B. P. Dailey, *J. Magn. Reson.* **12,** 36 (1973).

*45.* J. Vaara, K. Oikarinen, J. Jokisaari, and J. Lounila, *Chem. Phys. Lett.* **253,** 340 (1996).

*46.* M. H. Levitt and L. Di Bari, *Phys. Rev. Lett.* **69,** 3124 (1992).

*47.* G. Jaccard, S. Wimperis, and G. Bodenhausen, *Chem. Phys. Lett.* **138,** 601 (1987).

*48.* Z. Zheng, C. L. Mayne, and D. M. Grant, *J. Magn. Reson. A* **103,** 268 (1993).